

7. J. C. Bradley, Z. M. Ma, S. G. Stephens, *Adv. Mater.* **11**, 374 (1999).
8. N. Bowden, A. Terfort, J. Carbeck, G. M. Whitesides, *Science* **276**, 233 (1997).
9. T. L. Breen, J. Tien, S. R. J. Oliver, T. Hadzic, G. M. Whitesides, *Science* **284**, 948 (1999).
10. J. D. Holmes, K. P. Johnston, R. C. Doty, B. A. Korgel, *Science* **287**, 1471 (2000).
11. T. Thurn-Albrecht *et al.*, *Science* **290**, 2126 (2000).
12. Y. Huang, X. F. Duan, Q. Q. Wei, C. M. Lieber, *Science* **291**, 630 (2001).
13. Y. Cui, Q. Q. Wei, H. K. Park, C. M. Lieber, *Science* **293**, 1289 (2001).
14. P. J. A. Kenis, R. F. Ismagilov, G. M. Whitesides, *Science* **285**, 83 (1999).
15. R. Pethig, Y. Huang, X. B. Wang, J. P. H. Burt, *J. Phys. D Appl. Phys.* **25**, 881 (1992).
16. G. Fuhr *et al.*, *Naturwissenschaften* **81**, 528 (1994).
17. T. Müller *et al.*, *J. Phys. D Appl. Phys.* **29**, 340 (1996).
18. O. D. Velev, E. W. Kaler, *Langmuir* **15**, 3693 (1999).
19. R. Pethig, *Crit. Rev. Biotechnol.* **16**, 331 (1996).
20. The gold suspensions were prepared (34) at an Au concentration of 0.01 weight %. The mean size of the particles was determined by dynamic light scattering. The gold suspension was washed three times and concentrated to ~1.5 weight % by centrifugation through a 5000 molecular weight membrane.
21. T. B. Jones, *Electromechanics of Particles* (Cambridge Univ. Press, Cambridge, 1995).
22. H. A. Pohl, *Dielectrophoresis* (Cambridge Univ. Press, Cambridge, 1978).
23. A. P. Gast, C. F. Zukoski, *Adv. Colloid Interface Sci.* **30**, 153 (1989).
24. M. Trau, S. Sankaran, D. A. Saville, I. A. Aksay, *Nature* **374**, 437 (1995).
25. M. Dueweke, U. Dierker, A. Hübler, *Phys. Rev. E* **54**, 496 (1996).
26. W. J. Wen, K. Q. Lu, *Phys. Rev. E* **55**, R2100 (1997).
27. The energy of interaction between two closely situated polarizable particles can be approximated by  $W_{\max} = -C\pi\epsilon R^3 K^2 E^2 / r^3$ , where  $R$  is the particle radius,  $r$  the distance between the centers,  $E$  the intensity of the field, and  $\epsilon$  the dielectric permittivity of the media. The Clausius-Mossotti function,  $K$ , for metallic particles is  $\approx 1$  and the factor  $C$  ranges from 8 to more than hundreds, depending on the distance between the particles, the higher-order multipolar effects, and the number of particles in a chain (21, 22). Even for values of  $C$  above 1000, the estimated interaction energy between nanoparticles is smaller than  $10^{-2} kT$  ( $kT$  being the thermal energy).
28. Supplementary Web material is available on Science Online at [www.sciencemag.org/cgi/content/full/294/5544/1082/DC1](http://www.sciencemag.org/cgi/content/full/294/5544/1082/DC1).
29. The microwire fractal dimensions ranged from 1.01 to 1.71. The Hausdorff dimensions were calculated by computing the density-density correlation function from digitized pictures of the microwires (35), assuming that the narrow chamber restricts the growth to two dimensions. At higher voltages, segment rearrangement during growth yields microwires of lower dimension.
30. Rough estimates of the mechanical properties of the microwires are given by their response to the viscous flow of liquid in the flow cell. The wires remain intact after thousands of load/unload cycles of pulsing liquid flow. In addition, the application of voltage between the electrodes immediately restores snapped wires.
31. Any porous conglomerate of gold particles can be expected to display similar changes in resistivity because of surface functionalization (36). However, the microwires provide a number of advantages as compared with, for example, deposited strips of gold particles. The wires have more efficient mass transfer, provide sampling through the bulk of the liquid rather than on a surface, can be made as small as necessary, and are formed and automatically interconnected by self-assembly, rather than mask deposition or microprinting.
32. C. D. Bain *et al.*, *J. Am. Chem. Soc.* **111**, 321 (1989).
33. R. R. Shah, N. L. Abbott, *Science* **293**, 1296 (2001).
34. J. W. Slot, H. J. Geuze, *Eur. J. Cell Biol.* **38**, 87 (1985).
35. M. Matsushita, M. Sano, Y. Hayakawa, H. Honjo, Y. Sawada, *Phys. Rev. Lett.* **53**, 286 (1984).
36. C. Z. Li, H. Sha, N. J. Tao, *Phys. Rev. B* **58**, 6775 (1998).
37. This work was supported by the National Science Foundation (grant CTS-9986305). The critical comments and support of A. Lenhoff and R. Lobo are gratefully acknowledged. J.P.W. participated in this

work as a summer research student from the Department of Chemical Engineering, Carnegie Mellon University (Pittsburgh, PA), and was supported by the NSF (REU grant EEC-9820322).

26 June 2001; accepted 28 September 2001

## Oscillations in Phanerozoic Seawater Chemistry: Evidence from Fluid Inclusions

Tim K. Lowenstein,<sup>1\*</sup> Michael N. Timofeeff,<sup>1</sup> Sean T. Brennan,<sup>1</sup> Lawrence A. Hardie,<sup>2</sup> Robert V. Demicco<sup>1</sup>

Systematic changes in the chemistry of evaporated seawater contained in primary fluid inclusions in marine halites indicate that seawater chemistry has fluctuated during the Phanerozoic. The fluctuations are in phase with oscillations in seafloor spreading rates, volcanism, global sea level, and the primary mineralogies of marine limestones and evaporites. The data suggest that seawater had high  $Mg^{2+}/Ca^{2+}$  ratios ( $>2.5$ ) and relatively high  $Na^+$  concentrations during the Late Precambrian [544 to 543 million years ago (Ma)], Permian (258 to 251 Ma), and Tertiary through the present (40 to 0 Ma), when aragonite and  $MgSO_4$  salts were the dominant marine precipitates. Conversely, seawater had low  $Mg^{2+}/Ca^{2+}$  ratios ( $<2.3$ ) and relatively low  $Na^+$  concentrations during the Cambrian (540 to 520 Ma), Silurian (440 to 418 Ma), and Cretaceous (124 to 94 Ma), when calcite was the dominant nonskeletal carbonate and K-, Mg-, and Ca-bearing chloride salts, were the only potash evaporites.

The long-held consensus that the major-ion chemistry ( $Na^+$ ,  $K^+$ ,  $Ca^{2+}$ ,  $Mg^{2+}$ ,  $Cl^-$ ,  $SO_4^{2-}$ ,  $HCO_3^-$ ) of the global ocean has remained close to its present-day composition during the Phanerozoic (1) (~540 Ma to the present) is at odds with the record of secular changes in the primary mineralogy of marine limestones and evaporites. During the Phanerozoic, the primary mineralogy of nonskeletal limestones has twice oscillated between calcite and aragonite seas (2), while over the same interval of 540 million years (My), late-stage salts in marine evaporites have fluctuated between the KCl and  $MgSO_4$  types, in step with the calcite-aragonite oscillations (3). Current hypotheses for these 100- to 200-My cycles in limestone and evaporite mineralogies involve secular variation in the major-ion chemistry of seawater produced by changes in mid-ocean ridge hydrothermal brine fluxes driven by oscillations in seafloor spreading rates (3), as well as seawater-driven dolomitization (4). Here, we evaluate secular changes in seawater chemistry in the Phanerozoic through analysis of fluid inclusions.

Bedded halite from marine evaporites as old as the Late Precambrian contains preserved

“chevron” crystals formed by primary precipitation on the floor of an evaporating brine body (5). These chevron crystals contain bands of primary fluid inclusions parallel to the crystal growth faces, indicating that the inclusions hold trapped surface brines. Individual fluid inclusions in chevron halite are difficult to analyze by extraction techniques because of their dense packing and small size. This problem was overcome by using a scanning electron microscope (SEM) coupled to an x-ray energy-dispersive system (EDS) to directly analyze the major ions in frozen fluid inclusions as small as 30  $\mu m$  (6). An improved SEM-EDS approach using an environmental SEM (ESEM-EDS) allows direct observation and analysis of the surface of frozen fluid inclusions (7). Here, we present new ESEM-EDS analyses of fluid inclusions from Late Precambrian, Cambrian, Silurian, Permian, Cretaceous, and modern halites (8). Our data are from chevron halites that appear petrographically to be primary (i.e., unrecrystallized). We supplemented our data with published Permian (9, 10) and Tertiary (11) fluid inclusion analyses.

Fluid inclusions from halites (Fig. 1) trace out paths on  $Mg^{2+}$  and  $Na^+$  versus Cl plots that reflect changes in brine composition consistent with progressive evaporative concentration in the halite field. Such brine evolution paths support the textural evidence that the inclusions analyzed were trapped during various stages of evaporation of surface brines and not during burial. None of the ancient fluid inclusions, or the evaporation paths they define,

<sup>1</sup>Department of Geological Sciences and Environmental Studies, State University of New York, Binghamton, NY 13902, USA. <sup>2</sup>Department of Earth and Planetary Sciences, Johns Hopkins University, Baltimore, MD 21218, USA.

\*To whom correspondence should be addressed. E-mail: lowenst@binghamton.edu

## REPORTS

overlap the modern seawater evaporation curves or present-day fluid inclusions (Fig. 1). We interpret this to indicate that ancient seawater differed chemically from present-day seawater. Ancient fluid inclusion chemistries and paleo-evaporation paths form two distinct compositional groups: a Late Precambrian and Permian group, which is closest to modern seawater chemistry, and a Cambrian, Silurian, and Cretaceous group, which plots furthest from modern seawater evaporation paths. The  $\text{Na}^+$  versus  $\text{Cl}^-$  plot shows that ancient fluid inclusions had lower  $\text{Na}^+$  concentrations and higher  $\text{Cl}^-$  concentrations during halite precipitation than in present-day halite-saturated seawater brines. The  $\text{Mg}^{2+}$  versus  $\text{Cl}^-$  plot shows that paleoseawaters were depleted in  $\text{Mg}^{2+}$  relative to present-day evaporated seawater, with Late Precambrian and Permian fluid inclusions closest to modern concentrations.

The  $\text{Mg}^{2+}/\text{Ca}^{2+}$  molar ratio of paleoseawater estimated from fluid inclusions in halite spanning the Phanerozoic shows systematic long-term (100 to 200 My) oscillations (Fig. 2). Cambrian, Silurian, and Cretaceous paleoseawaters had maximum  $\text{Mg}^{2+}/\text{Ca}^{2+}$  ratios of 2.3 and ranges between 1.0 and 2.3, well below the modern seawater  $\text{Mg}^{2+}/\text{Ca}^{2+}$  ratio of 5.2 (12).  $\text{Mg}^{2+}/\text{Ca}^{2+}$  ratios in Late Precambrian, Permian, and Tertiary seawater were decidedly higher, always  $>2.5$  and at times  $>4$  (13). Variations in the  $\text{Mg}^{2+}/\text{Ca}^{2+}$  ratio of seawater are synchronous with variations in  $\text{Na}^+$  and  $\text{Mg}^{2+}$ . Geological periods during which seawater had high ( $>2$ )  $\text{Mg}^{2+}/\text{Ca}^{2+}$  ratios (Late Precambrian, Permian, and Tertiary) coincided with times of relatively elevated  $\text{Mg}^{2+}$  and  $\text{Na}^+$  concentrations, and they correspond to periods when aragonite and  $\text{MgSO}_4$  salts were important marine precipitates (Fig. 2). The high  $\text{Mg}^{2+}/\text{Ca}^{2+}$  ratio of seawater was probably responsible for the precipitation of aragonite during those times, in accord with field and experimental evidence that aragonite is the favored carbonate to precipitate from waters with  $\text{Mg}^{2+}/\text{Ca}^{2+}$  ratios  $> \sim 2$  (3, 14).  $\text{MgSO}_4$ -bearing salts such as polyhalite, kainite, and kieserite occur in Permian and Tertiary evaporites. During these periods, seawater fell on the  $\text{SO}_4^{2-}$ -rich side of the  $\text{Ca-SO}_4$  chemical divide (13), and  $\text{Ca}^{2+}$ -depleted,  $\text{SO}_4^{2-}$ -rich brines were produced after precipitation of  $\text{CaCO}_3$  and  $\text{CaSO}_4$ . In contrast, seawater with low  $\text{Mg}^{2+}/\text{Ca}^{2+}$  ratios ( $<2.3$  in the Cambrian, Silurian, and Cretaceous) coincided with times when seawater was relatively depleted in  $\text{Na}^+$  and  $\text{Mg}^{2+}$ . Calcite was the dominant nonskeletal carbonate of these periods, which is consistent with observations that low-Mg calcite is the favored carbonate to precipitate from waters with  $\text{Mg}^{2+}/\text{Ca}^{2+}$  ratios  $< \sim 2$ . Cambrian, Silurian, and Cretaceous evaporites lack  $\text{MgSO}_4$  minerals and instead contain late-stage K-, Mg-, and Ca-bearing chloride salts. Seawater of these ages must have had relatively elevated  $\text{Ca}^{2+}$  with molal (m) concen-

trations of  $m\text{Ca}^{2+} > m\text{SO}_4^{2-} + \frac{1}{2}m\text{HCO}_3^-$ , which ensured that  $\text{Ca}^{2+}$  would become a major brine component, and  $\text{SO}_4^{2-}$  a minor brine component, after evaporation and precipitation of  $\text{CaSO}_4$ .

The fluid inclusion data (Figs. 1 and 2) provide evidence for oscillations in the major-ion chemistry of seawater over the Phanerozoic. The oscillations in seawater composition are of the kinds predicted by a seawater secular variation model (3), which proposes that secular changes in seawater chemistry are produced by changes in the mid-ocean ridge/river water flux

ratio driven by changes in ocean crust production (15). The data are also in good agreement with the timing of aragonite and calcite seas and with the observed occurrences of  $\text{MgSO}_4$ -rich versus KCl-rich potash evaporites back at least to the Late Precambrian. During geologic periods with high mid-ocean ridge activity and high sea levels (Cambrian, Silurian, and Cretaceous), substantial changes in the chemistry of seawater are predicted, even the crossing of the  $\text{Ca-SO}_4$  chemical divide. Seawaters from those periods, with  $m\text{Ca}^{2+} > m\text{SO}_4^{2-} + \frac{1}{2}m\text{HCO}_3^-$ , would have evolved after evaporation and precipitation

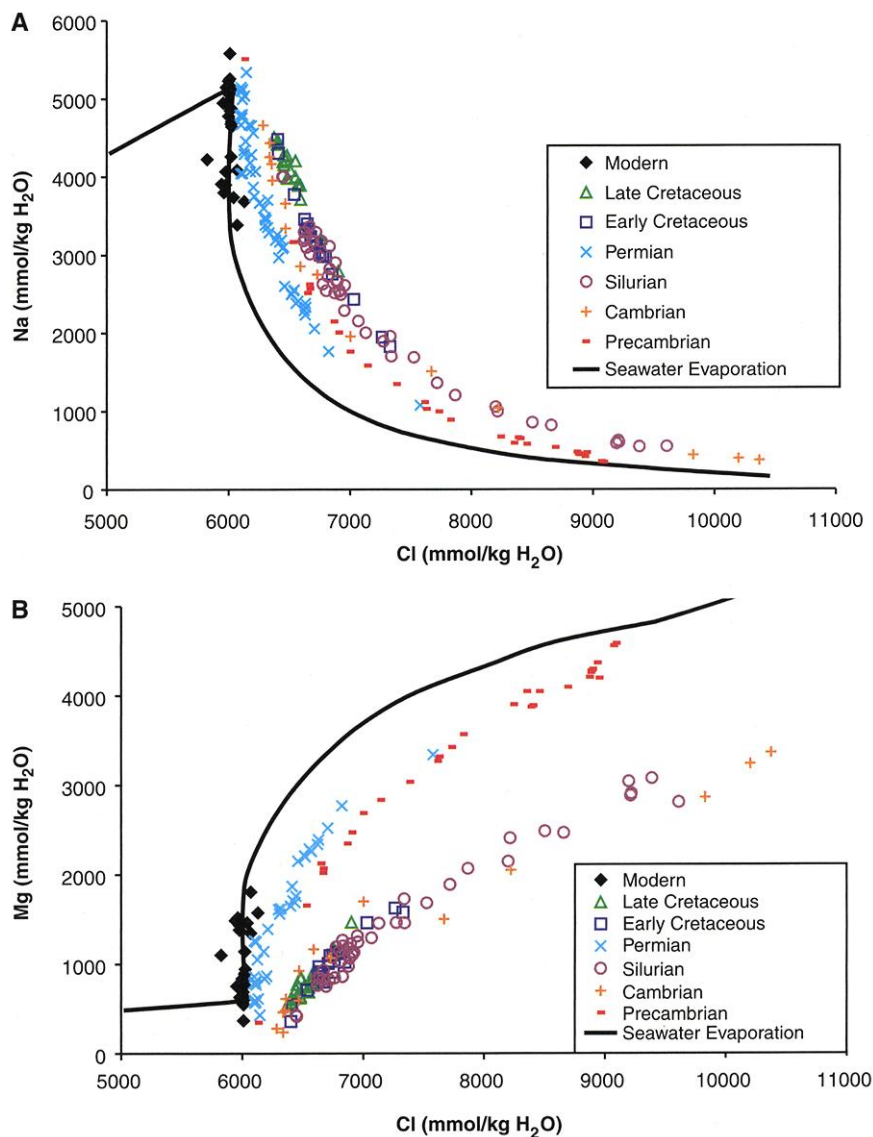


**Fig. 1.** Concentrations of  $\text{Na}^+$  (A) and  $\text{Mg}^{2+}$  (B) versus  $\text{Cl}^-$  in primary fluid inclusions from marine halites (8), analyzed by ESEM-EDS. Permian fluid inclusions analyzed by extraction-ion chromatography (9) and extraction-microtitration (10) are also plotted. Solid curves track the compositional paths for evaporation of modern seawater calculated by the HMW computer program (18). Evaporation paths are functions of the major-ion chemistry of the parent water, the extent of evaporation, and the type and amount of salts precipitated. Fluid inclusions from present-day marine halites overlap the modern seawater evaporation paths, indicating that fluid inclusions from modern halites contain unaltered evaporated seawater brines (19). The drop in  $\text{Na}^+$  and increase of  $\text{Mg}^{2+}$  on the modern seawater evaporation curves at  $\sim 6000$  mmol of  $\text{Cl}^-$  reflect precipitation of halite and loss of  $\text{Na}^+$  and  $\text{Cl}^-$  from the evaporating brines.  $\text{Na}^+$  and  $\text{Cl}^-$  molalities from all fluid inclusions were adjusted using the HMW computer model assuming halite saturation.

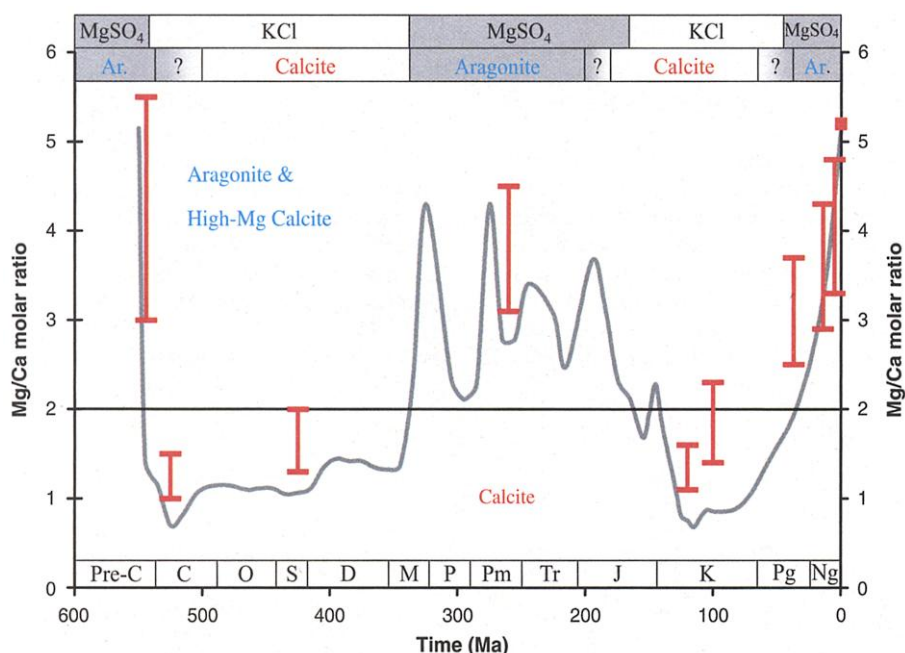


**Fig. 2.** Secular variation in the  $Mg^{2+}/Ca^{2+}$  ratio of seawater during the Phanerozoic, estimated from fluid inclusions in marine halites (vertical bars) (12, 13) compared to predicted seawater secular variations (3). The horizontal line at  $Mg^{2+}/Ca^{2+} = 2$  is the approximate divide between calcite seas ( $Mg^{2+}/Ca^{2+} < 2$ ) and aragonite seas ( $Mg^{2+}/Ca^{2+} > 2$ ) (3, 17). Also plotted are the temporal distributions in the primary mineralogies of Phanerozoic nonskeletal carbonates (2) and KCl and  $MgSO_4$  evaporites (3).

of  $CaSO_4$  into the  $Ca^{2+}$ -rich  $SO_4^{2-}$ -depleted fluid inclusions reported here. In this regard, it is likely that the overall slowdown in seafloor spreading rates since the Cretaceous maximum ultimately led to a present-day seawater chemistry at the other chemical extreme, enriched in  $SO_4^{2-}$ ,  $Mg^{2+}$ , and  $Na^+$  and depleted in  $Ca^{2+}$ .

We interpret these data to indicate that the major-ion chemistry of seawater has systematically changed over the last 540 My. However, others have suggested that any such signal may be obscured by basinal- or global-scale dolomitization of flooded carbonate platforms, which altered the  $Mg^{2+}/Ca^{2+}$  ratio of the evaporating brines, yielding seawater enriched in  $Ca^{2+}$  and depleted in  $Mg^{2+}$  (4). If basinal-scale contemporaneous dolomitization were to have altered seawater chemistry before evaporative concentration, then we would not expect overlapping fluid inclusion chemistries in samples taken from geographically separated evaporite basins of about the same age (Fig. 1). It is noteworthy that fluid inclusions analyzed from the Silurian, Permian, and Cretaceous came from geographically separate areas (8). Such overlaps indicate a common "global" seawater parent of that period. Global-scale dolomitization during periods of elevated sea level (e.g., the Cretaceous) could produce seawater enriched in  $Ca^{2+}$  and relatively depleted in  $Mg^{2+}$ , as observed. However, the systematic changes in the  $Na^+$  concentration of fluid inclusions (Fig. 1) cannot be explained by dolomitization. We conclude that some of the observed scatter of the fluid inclusion data may have been pro-

duced by contemporaneous dolomitization of marine limestones, but that changes in the chemistry of evaporating seawater produced by these processes were not large enough to override the basic seawater signal.

Long-term changes in seafloor spreading rates, global sea level, and "greenhouse" versus "icehouse" conditions are synchronous during the Phanerozoic because they are all driven by plate tectonics, as pointed out in 1982 (16). To this list we would add oscillations in global seawater chemistry recorded in the minerals (and their fluid inclusions) of marine evaporites and nonskeletal limestones. Changes in the major-element chemistry of ancient seawater may also have influenced the mineralogy and abundance of the dominant biocalcifying organisms in the past. This is suggested by the concurrence of the carbonate mineralogy (aragonite versus calcite) of many "dominant" reef builders and sediment-producing organisms (17) with the fluctuations in the chemistry of seawater reported here.

**References and Notes**

1. W. W. Rubey, *Bull. Geol. Soc. Am.* **62**, 1111 (1951).
2. P. A. Sandberg, *Nature* **305**, 19 (1983).
3. L. A. Hardie, *Geology* **24**, 279 (1996).
4. H. D. Holland, H. Zimmermann, *Int. Geol. Rev.* **42**, 481 (2000).
5. T. K. Lowenstein, L. A. Hardie, *Sedimentology* **32**, 627 (1985).
6. C. Ayora, J. Garcia-Veigas, J. J. Pueyo, *Geochim. Cosmochim. Acta* **58**, 3379 (1994).
7. M. N. Timofeeff, T. K. Lowenstein, W. H. Blackburn, *Chem. Geol.* **164**, 171 (2000).
8. Samples analyzed by ESEM-EDS: Late Precambrian (543 to 544 Ma), Ara Group, Oman; Early Cambrian

- (520 to 540 Ma), Angarskaya Formation (Fm.), Siberia; Silurian (418 to 440 Ma), Salina Group, Michigan, USA, and Carribuddy Group, Western Australia; Permian (251 to 258 Ma), Salado Fm., New Mexico, USA; Early Cretaceous (112 to 124 Ma), Muribeca Fm., Brazil, and Loeme Fm., Congo; Late Cretaceous (94 to 112 Ma), Maha Sarakham Fm., Laos-Thailand; modern halite, Baja California, Mexico.

9. J. Horita, T. J. Friedman, B. Lazar, H. D. Holland, *Geochim. Cosmochim. Acta* **55**, 417 (1991).
10. T. M. Peryt, V. M. Kovalevich, *Zbl. Geol. Palaeont. Teil I* **1995**, 337 (1996).
11. H. Zimmermann, *Am. J. Sci.* **300**, 723 (2000).
12. Maximum paleoseawater  $Mg^{2+}/Ca^{2+}$  ratios for the Cambrian, Silurian, and Cretaceous (Fig. 2, top of vertical bars) were found directly by ESEM-EDS measurement of  $Mg^{2+}$  and  $Ca^{2+}$  in fluid inclusions [analytical accuracy, (mean - expected)/expected, is better than 7%; precision (relative standard deviation) is 6% for  $Ca^{2+}$  and 16% for  $Mg^{2+}$ ]. Measured  $Mg^{2+}/Ca^{2+}$  ratios are maxima because they do not account for the  $Ca^{2+}$  lost from seawater during earlier precipitation of  $CaCO_3$  and  $CaSO_4$ , formed before halite.  $Mg^{2+}/Ca^{2+}$  ratios in Cambrian, Silurian, and Cretaceous paleoseawater were also modeled using the Harvie-Møller-Weare (HMW) computer program (18) (bottom of vertical bars). Because the analyzed fluids are concentrated brines, we used the following backtracking procedure to estimate the compositions of the parent seawaters. Measured concentrations of the individual major ions in the inclusion fluids were plotted against the conservative ion  $Mg^{2+}$ , the progress variable of evaporative concentration, which does not partition into solid phases until the late "bit-tern" stages. We then used the HMW computer program to determine, for each evaporite deposit examined, the paleoseawater with the major-ion composition that provided the best fit to the full set of  $Na^+$ ,  $K^+$ ,  $Ca^{2+}$ , and  $Cl^-$  versus  $Mg^{2+}$  plots, using trial-and-error fitting. A requirement of the modeling procedure was that the succession of salts formed from evaporation of modeled paleoseawater of a given age exactly match the observed sequence of evaporites. All modeling was done using a present-day  $Cl^-$  of 548 mmol and assuming that  $SO_4^{2-}$  was 14 mmol; present-day  $SO_4^{2-}$  is 28 mmol.
13.  $Mg^{2+}/Ca^{2+}$  ratios in Precambrian and Permian seawater could not be obtained directly from fluid inclusions because they contained no measurable  $Ca^{2+}$  and therefore fell on the  $SO_4^{2-}$  side of the  $Ca$ - $SO_4$  chemical divide, as does modern seawater. In these waters, evaporation and precipitation of  $CaCO_3$  and  $CaSO_4$  consumes virtually all  $Ca^{2+}$  from the brines, leaving  $SO_4^{2-}$  in excess during later brine evolution. For these geological periods, we estimated the seawater  $Mg^{2+}/Ca^{2+}$  ratios by the modeling procedures outlined in (12), assuming  $Ca^{2+}$  of 10 mmol ( $Ca^{2+}$  concentration in modern seawater giving the maximum  $Mg^{2+}/Ca^{2+}$  on vertical bars) and a  $Ca^{2+}$  of 15 mmol, 1.5 times modern seawater (minimum  $Mg^{2+}/Ca^{2+}$  on vertical bars). The three Tertiary  $Mg^{2+}/Ca^{2+}$  ratios were calculated from the  $Mg^{2+}$  concentrations of (17) for Eocene (37 Ma), Middle Miocene (14 Ma), and Late Miocene (5 Ma) paleoseawater, and  $Ca^{2+}$  concentrations of 10 and 15 mmol.
14. J. W. Morse, Q. Wang, M. Y. Tsio, *Geology* **25**, 85 (1997).
15. One limitation of the seawater secular variation hypothesis is the incomplete knowledge of ancient mid-ocean ridge hydrothermal brine fluxes.
16. A. G. Fischer, in *Climate in Earth History* (National Academy Press, Washington, DC, 1982), pp. 97-104.
17. S. M. Stanley, L. A. Hardie, *GSA Today* **9** (no. 2), 1 (1999).
18. C. E. Harvie, N. Møller, J. H. Weare, *Geochim. Cosmochim. Acta* **48**, 723 (1984). The HMW computer program calculates, at each evaporation step, concentrations (in molalities) of all the major ions and moles of salts precipitated.
19. M. N. Timofeeff et al., *Geochim. Cosmochim. Acta* **65**, 2293 (2001).
20. We thank W. Blackburn for laboratory assistance, and N. Harris, R. Hite, J. Horita, V. Kovalevich, M. A. da Silva, M. El Tabakh, and H. Zimmermann for samples and discussions. Supported by NSF grant EAR-9725740.

11 July 2001; accepted 19 September 2001